Hole spin dynamics under π pulse excitation

A. Dargys*

Semiconductor Physics Institute, A. Goštauto 11, 2600 Vilnius, Lithuania

(Received 9 February 2004; revised manuscript received 6 July 2004; published 21 September 2004)

The control and dynamical properties of the valence-band hole spin in tetrahedral semiconductors subjected to an ultrashort π-type electric field pulse are presented. Using a concept of the hole spin surface [Phys. Status Solidi B **241**, 145 (2004)], it is shown that the control of spin of a ballistic hole having a well-defined wave vector and energy may be treated as the transitions between heavy, light, and split-off spin surfaces. Two types of spin transitions that are closely related to interband and intraband transfers of holes are introduced to explain the evolution of spin during excitation of holes by electrical π pulses. Numerical experiments using real valence bands of silicon are presented which show that the intervalence transitions due to interband tunneling give the largest contribution in the hole spin switching dynamics.

I. INTRODUCTION

There is a growing interest in the spintronics where both electron spin and charge are important in the operation of solid-state devices.[1–3] Most of the investigations performed until now were devoted to conduction-band electrons, since the lifetime of the electron spin is comparatively long: the spin memory is lost after 100 or more electron collisions with phonons or point impurities.[4–6] In contrast, the relaxation time of the hole spin is short. Due to the large spin-orbit coupling in the valence-band of elementary, III-V, and other compound semiconductors, the hole lifetime was found to be comparable to hole momentum scattering time.[7–10] Nonetheless, as we shall see, a coherent control of the hole spin degrees of freedom appears feasible, if the exciting pulse duration is shorter than hole momentum scattering time.

On the other hand, a richer spectrum of the spin states in the valence-band, where both $\frac{3}{2}$ and $\frac{1}{2}$ multiplets come into play, is expected to yield a richer physics. The valence band has three distinct spin surfaces related to three valence subbands.[11] It was found that in high-symmetry directions the spin states of heavy-mass holes depend on a single parameter only and, therefore, all possible average spins lie on a line rather than on a two-parameter spin surface. The spin states of the heavy hole, thus, appear to be more degenerate than those of other bands. At high hole energies the shape of the spin surfaces depends on the hole propagation direction and magnitude of the wave vector. By this reasoning the switching between heavy-mass and light-mass spin states is expected to be more complex than the switching of the conduction electron spin between $\pm\frac{1}{2}$ spin states. The latter switching, as known, occurs on the same spin surface.

Some preliminary results on hole spin switching dynamics by electric field for an idealized case (spherical and parabolic energy bands) were considered recently in Refs. 12 and 13. Here, a more realistic situation is considered, where three nonspherical and warped valence-bands—heavy-mass, light-mass, and spin-orbit split-off—are taken into account simultaneously. Since in the numerical analysis of hole dynamics the initial conditions for a wave function in the Schrödinger

equation should be known, in Sec. II the conditions appropriate to valence-band holes are discussed briefly at first. In Secs. III and IV spin switching by relatively long and harmonically varying π-type electric field pulses under resonance and off-resonance conditions is considered. For this purpose the Schrödinger equation was solved numerically using the valence-band parameters of silicon. In Sec. V the results on spin switching by ultrashort and optimized pulses are described. In Sec. VI the differences between electron and hole spin switching dynamics are discussed and conclusions are drawn. The analysis is restricted to a single hole, with the aim of capturing the physics of how a coherent switching of the hole spin under low- and high-intensity excitation takes place. By the same motive the spin relaxation is not considered in this paper. In realistic situations, where the relaxation is important, the simulation of transient spin processes should be done using the hole density matrix.[14]

II. INITIAL CONDITIONS FOR HOLE SPIN AND EQUATIONS SOLVED

In the angular momentum representation, the valence band of elementary semiconductors is described by the Luttinger-Kohn Hamiltonian.[15,16] Due to strong spin-orbit interactions in the valence band, the total angular momentum operator **J**, which for brevity will be referenced in this paper as the hole spin operator, in general, does not commute with the Luttinger-Kohn Hamiltonian. Physically this means that the hole spin is not a good quantum number for a hole moving ballistically in a particular energy band. In the angular momentum representation the operator **J** for heavy-mass, light-mass, and split-off bands consists of a direct sum of $\frac{3}{2}$ and $\frac{1}{2}$ spin operators. In the simulation it was assumed that before application of the electric field, at the moment $t=0$, the hole was in one of the bands and its wave function $f_n(t=0,\mathbf{k}_0)$ was characterized by the wave vector $\mathbf{k}_0$ and the band index n. Thus, it is thought that at $t=0$ the hole has a well-defined energy $\varepsilon_n(\mathbf{k}_0)$.

As known, the energy bands of elementary semiconductors due to the presence of inversion symmetry are doubly degenerate. The degeneracy reflects two possible spin states.
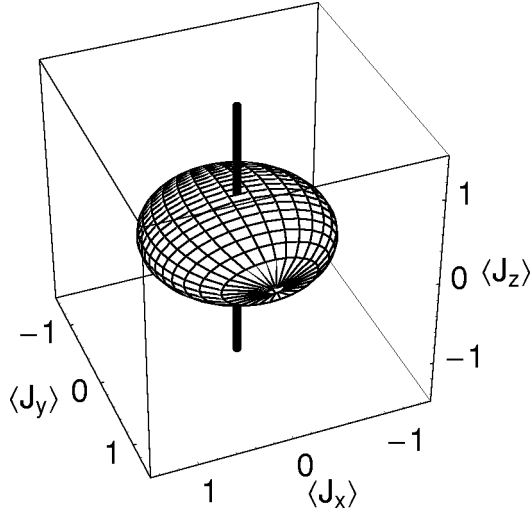
FIG. 1. Spin surfaces of heavy and light holes in the spherical and parabolic energy band approximation. For light holes the surface is the spheroid with principal axes $\langle J_z \rangle_{max} = \frac{1}{2}$ and $\langle J_x \rangle_{max} = \langle J_y \rangle_{max} = 1$. For heavy holes the spin surface degenerates to a line which is parallel to hole wave vector, $\langle \mathbf{J} \rangle \| \mathbf{k}$. The extreme values of spin in the latter case are $\langle J_z \rangle_{max} = \pm \frac{3}{2}$.

The doubly degenerate states can be described parametrically by two variables, in this paper denoted as a and ϕ. The parameter ϕ describes a relative phase, while a describes a contribution of one of the degenerate states in the superposition state. For example, if initially the hole is in the heavy-mass band, then the corresponding six-component spinor in the energy representation can be taken in the form

$$f_h = (a, e^{i\phi}\sqrt{1-a^2}, 0, 0, 0, 0), \qquad (1)$$

where $\phi = 0, \dots, 2\pi$ and $a = 0, \dots, 1$. The following order of bands was assumed in this paper $(f_h^{(+)}, f_h^{(-)}, f_l^{(+)}, f_l^{(-)}, f_s^{(+)}, f_s^{(-)})$, where the subscripts h, l, and s denote heavy-mass, light-mass, and split-off bands, and the superscripts $(+)$ and $(-)$ correspond to two degenerate spin states. The function (1) is normalized to unity. Similar superposition states can be written if the hole finds itself in light-mass or split-off band. As shown in Ref. 11 the parameters a and ϕ at the same time represent all possible spin states of holes on the spin surface embedded in the three-dimensional spin space. As an example, in Fig. 1 there are shown all possible states of total angular momentum

$$\langle \mathbf{J} \rangle_{h,l} = \langle f_{h,l} | \mathbf{J} | f_{h,l} \rangle \qquad (2)$$

of heavy and light holes that possess a vanishingly small wave vector $\mathbf{k}$ which is parallel to the [001] crystallographic axis. As shown in the Appendix, similar surfaces are found, if one considers spherical and parabolic two-, heavy-mass, and light-mass bands. The geodesic lines, which are tips of the average spin vectors $\langle \mathbf{J} \rangle_{h,l}$, correspond to fixed values of a and ϕ. Figure 1 shows that for light-mass holes the ends of the average spin lie on the spheroid, whose rotation axis is parallel to $\mathbf{k}$. The spin surface of the heavy-mass hole, in this approximation, has shrunk to a line. However, for real bands the spin degeneracy will be lifted and the spin line will trans-

form to a cigar-shaped spin surface [cf. Fig. 5(b)]. Figure 1 corresponds to a hole wave vector pointing in the [001] crystallographic direction. For other directions of $\mathbf{k}$ the spin surfaces should be rotated in the same way as $\mathbf{k}$, so that the heavy-mass hole spin line and the minor axis of the spheroid will remain parallel to $\mathbf{k}$ (for more details see the Appendix). If bands are warped and nonparabolic, the shape of the spin surface will also depend on the magnitude and direction of $\mathbf{k}$.[11] Thus, apart from the band index, the shape of the spin surface also, in a general case, will depend on hole propagation direction and velocity. The degree of distortion of spin surfaces reflects the degree of deviation of the energy bands from the spherical and parabolic model. Due to the small spin-orbit splitting energy Δ, especially strong distortions of the spin surfaces take place in silicon. The concept of a spin surface is very convenient in practical calculations because it allows one to determine the initial and final hole spin states in intraband and interband hole transitions. Since the initial wave function and the corresponding point on the spin surface are mutually related, the assumption about spin direction and spin magnitude is equivalent to the selection of concrete values of the parameters a and ϕ in the initial wave function for the Schrödinger equation—for example, in the vector (1). For real nonparabolic and warped valence bands, numerical precalculations are required to know the form of the spin surface at a given initial and final wave vector $\mathbf{k}$ and band index n. If the magnitude of $\mathbf{k}$ is not too large, formulas (A11)–(A16) in the Appendix can be used for this purpose.

In this paper the spin dynamics and intervalence transitions were simulated by the following Schrödinger system of equations for the six-component spinor $|\psi\rangle$ in the effective mass approximation:

$$i\hbar \frac{\partial |\psi\rangle}{\partial t} = [H_{LK}(\mathbf{k}) + H_F(\mathbf{k})]|\psi\rangle, \qquad (3)$$

where $i = \sqrt{-1}$ and $\hbar$ is the Planck constant. $H_{LK}(\mathbf{k})$ is the 6 × 6 Luttinger-Kohn Hamiltonian[15] and $H_F(\mathbf{k})$ is the field term. Using the equation of motion for the wave vector,

$$d\mathbf{k}/dt = (e/\hbar)\mathbf{F}(t), \qquad (4)$$

where $\mathbf{F}(t)$ is the time-dependent electric field, the Schrödinger equation (3) can be transformed from partial to total derivatives. The correct form of the field Hamiltonian $H_F(\mathbf{k})$ was given recently by Foreman in Ref. 17, where he has shown that in $H_F(\mathbf{k})$, along with the term that is proportional to electric field F_j, one must also include the terms proportional to $k_i F_j$ and F_j^3, where $i, j = x, y, z$. In the following only the leading term proportional to the electric field was retained:

$$H_F(\mathbf{k}) \approx \frac{e\mathbf{F}(t)}{i} \frac{\partial}{\partial \mathbf{k}}, \qquad (5)$$

where e is the elementary charge. Estimation of the higher-order terms in $H_F(\mathbf{k})$ shows that their contribution does not change qualitatively the results presented below.

The time dependence of the average spin projections was found from

$$\langle J_j \rangle_i = \langle \psi_i | J_j | \psi_i \rangle, \qquad (6)$$

where J_j is the jth component of the total 6×6 angular momentum matrix. The subscript j denotes the Cartesian component (x, y, or z) and the subscript i denotes a particular band ($i = h, l,$ or s). The concrete forms of the matrices J_j can be found in Ref. 11. To conform with the matrix structure of Refs. 15 and 16 in this paper J_x and J_y matrices were interchanged: $J_x \rightarrow -J_y$, $J_y \rightarrow J_x$. The numerical singular value decomposition of the Luttinger-Kohn Hamiltonian at a given wave vector $\mathbf{k}$ was used to connect the state vector $|\psi\rangle$ in the spinor representation to its partner in the energy band representation $|f\rangle$ for example, given by expression (1).

In the calculations, the valence-band parameters of silicon were used: $\gamma_1 = 4.22$, $\gamma_2 = 0.53$, $\gamma_3 = 1.38$, $\Delta = 0.0426$ eV. The representative wave vector was $k_{z0} = 0.378$ nm^{-1}, which gives the following energies: $\varepsilon_h = 17.2$ meV, $\varepsilon_l = 27.1$ meV, and $\varepsilon_s = 67.29$ meV. The nonsphericity parameter[18] of the silicon valence band is relatively large: $\delta = (\gamma_3 - \gamma_2)/\gamma_1 = 0.2$. This set gives relatively strong energy band anisotropy and nonparabolicity, which is reflected in hole spin properties too (see Sec. V).

III. RESONANCE EXCITATION

Figures 2 and 3 show time dependence of the probabilities p_n, where $n = h, l,$ or s, to find the hole in all three valence bands and the evolution of Cartesian spin components under pulsed and circularly polarized π-type excitation having Gaussian envelope. Initially the hole was placed in the heavy-mass band with wave vector $\mathbf{k}_0$ parallel to [001] axis. The frequency ω of the exciting pulse was set to resonance: $\hbar\omega = \Delta\varepsilon_{hl}(\mathbf{k}_0) = \varepsilon_l(\mathbf{k}_0) - \varepsilon_h(\mathbf{k}_0) = 9.89$ meV for the heavy-light transition in Fig. 2 and $\hbar\omega = \Delta\varepsilon_{hs}(\mathbf{k}_0) = \varepsilon_s(\mathbf{k}_0) - \varepsilon_h(\mathbf{k}_0) = 50.1$ meV for the heavy–split-off transition in Fig. 3. As seen from the figures, the π pulse transfers the hole from heavy-mass to either light-mass or split-off band with the probability p_l or p_s equal 1. The hole transfer and the switching of $\langle J_z \rangle$ component from $\langle J_z \rangle = -3/2$ to $-1/2$ is smooth when the field $\mathbf{F}$ is rotating counterclockwise, from F_x to F_y in the k_x-k_y plane. If instead of circular polarization a linear polarization was used, the time dependence of $\langle J_z \rangle$ and p_n assumed stepped character with period π/ω. Stronger electric fields were required in the latter case to reach $p_l = 1$ or $p_s = 1$ at the end of the pulse. For the opposite sense—that is, a clockwise rotation of the field—the excitation to l and s bands and the spin switching did not occur. Thus, Figs. 2 and 3 are examples of allowed and optimized spin intervalence transitions that were realized by selecting particular values of the parameters a and ϕ in the initial wave function (1). In the experiment, the initial spin is determined by a spin injector that establishes a nonequilibrium spin population. The properties of the injector here are played by the parameters a and ϕ.

Figures 2 and 3 represent the elementary spin control process between the two eigenstates of the system, where one of the spin components experiences smooth passage between $-\frac{3}{2}$ and $-\frac{1}{2}$ spin states, while the remaining components experience transient oscillations. In the numerical experiment
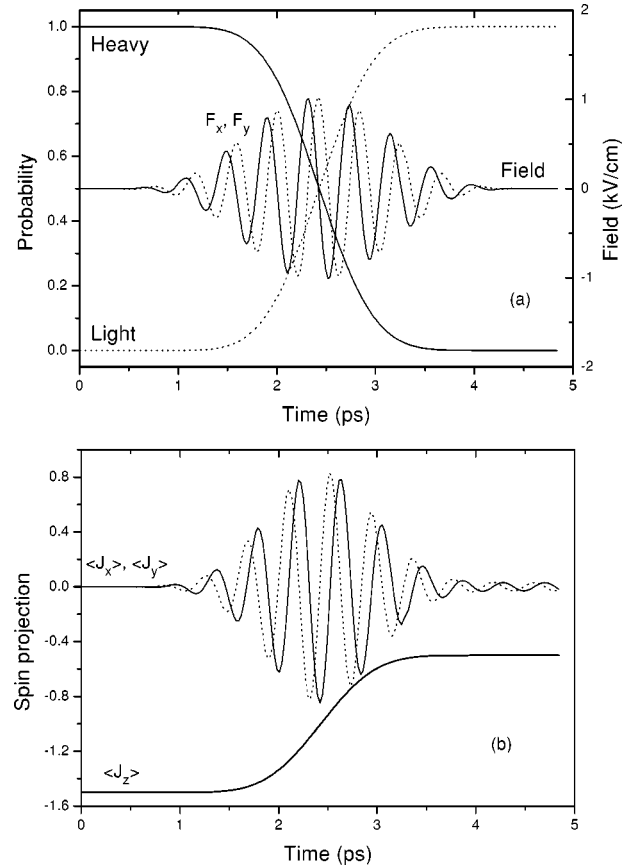

FIG. 2. (a) F_x and F_y components of the circularly polarized π-type electric pulse and time dependence of the probability to find the hole in the heavy- and light-mass bands. The frequency is tuned to the heavy-light resonance transition, $\hbar\omega = 9.89$ meV. (b) Time dependence of spin components excited by field shown in (a). The initial hole spin is $\langle \mathbf{J} \rangle = (0, 0, -3/2)$. $\mathbf{k}_0 \| [001]$.

this was achieved in two steps. At first, the electric pulse was optimized to obtain maximum interband transition probability p_l or p_s, and then the parameters a and ϕ in the spinor (1) were optimized to get the largest initial value of $\langle J_z \rangle$ on the spin line or surface.

In Fig. 4 there is shown the evolution of the spin projections when $\mathbf{k}_0 \| [111]$ and the electric field is linearly $[(F_{x\,max}: F_{y\,max}: F_{z\,max}) = (-4.5 : 1.15 : 3.3) \text{kV/cm}]$ polarized. The field is perpendicular to the wave vector, $\mathbf{F}(t) \perp \mathbf{k}_0 \| \langle \mathbf{J} \rangle$. The initial projections of $\langle \mathbf{J} \rangle$ in this case were (0.866, 0.866, 0.866); i.e., the parameters a and ϕ were selected so that the average spin vector was pointing in the [111] direction and its length was $\sqrt{\langle \mathbf{J} \rangle^2} = 1.5$. The exciting field was optimized to get the final population $p_l \simeq 1$. In comparing the results of Fig. 4 with those in Figs. 2 and 3 one should pay attention to the following points. After the excitation $t > 4$ ps, there is small precession of $\langle \mathbf{J} \rangle$ due to beating between light-hole and small residual heavy-mass hole wave functions. It was found that [111] spin is more sensitive to a small admixture of the wave functions of other bands. Second, in Figs. 2 and 3 the final and initial spins are parallel and point in the same direction. In Fig 4, however, the final spin is pointing in a different direction and makes the angle of 120° with $\mathbf{k}_0$. This
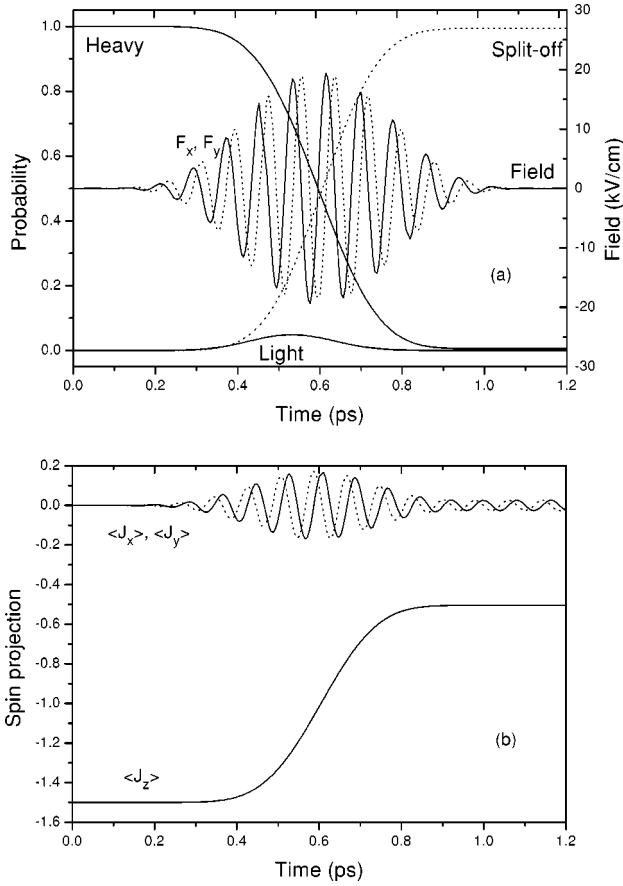
FIG. 3. The same as in Fig. 2 except that the laser was tuned to the heavy-mass–split-off resonance transition, $\hbar\omega = 50.1$ meV.

demonstrates that, in principle, one can control the direction of the spin by an electric field if intervalence excitation is induced by linearly polarized and specially tailored pulses.

Figure 5 illustrates the spin evolution of the hole that was propagating in an arbitrary direction, $\mathbf{k}_0 = (0.19, 0.28, 0.38)$ nm^{-1}, and was excited to the split-off band by a field circularly polarized in the k_x-k_y plane. The initial spin surface
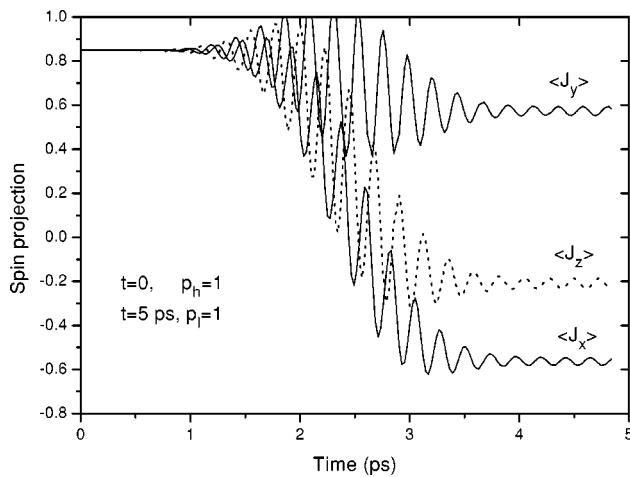

FIG. 4. Resonant heavy-light excitation of hole with $\mathbf{k}_0 \| \langle \mathbf{J} \rangle \| [111]$ by linearly polarized π-type pulse. $\hbar\omega = 18.5$ meV.
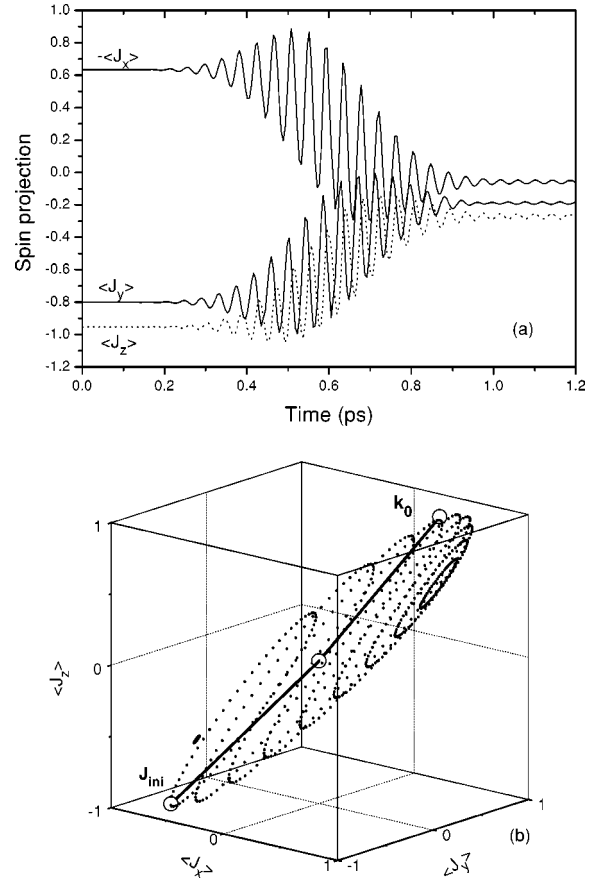

FIG. 5. (a) Resonant heavy-mass–split-off band excitation by π-type pulse, $\hbar\omega = 97.95$ meV, at randomly selected wave vector $\mathbf{k}_0 = (0.19, 0.28, 0.38)$ nm^{-1}. Note that in the figure the sign of $\langle J_x \rangle$ is opposite. (b) The corresponding heavy-hole spin surface represented by dotted geodesic lines. The direction of $\mathbf{k}_0$ and initial spin $\langle \mathbf{J} \rangle_{ini} = (-0.63, -0.8, -0.95)$ on the spin surface are shown by the open dots.

of a such hole has a cigar form, Fig. 5(b). The electric field amplitude and the initial projections of the heavy-mass hole spin, $\langle \mathbf{J} \rangle_{ini} = (-0.63, -0.8, -0.95)$, were selected so as to get maximal transfer of the hole to the split-off band, $p_{s \, max} = 0.994$. The reader should pay attention that now $\mathbf{k}_0$ and $\langle \mathbf{J} \rangle_{ini}$ are not parallel, more exactly, antiparallel, as one would expect for parabolic and spherical bands. They intersect at an angle of 174°. As is seen from Fig. 5, the magnitude of the final spin has reduced from $|\langle \mathbf{J} \rangle_{ini}| \simeq 1.5$ to $|\langle \mathbf{J} \rangle_{fin}| \simeq 0.36$. The small value of the final spin is associated with a small radius of the spin surface of the split-off band for real semiconductors. For spherical and parabolic bands the spin surface of the split-off band is a sphere of radius $\frac{1}{2}$.[11]

From this and the previous figures it can be concluded that the precession is not observed if a hole is transferred to either light-mass or split-off band with the probability equal or very close to 1. In such cases the final spin is determined by a point on the final spin surface of the respective band. However, if $p_l < 1$, the figures show that the precession frequency is equal or close to $\Delta\varepsilon_{hl}(\mathbf{k}_0)/\hbar$ or $\Delta\varepsilon_{hs}(\mathbf{k}_0)/\hbar$. Noting also that at the electric field intensities used the amplitude Δk of the time-dependent wave vector, according to Eq. (4), sat-

isfies the condition $\Delta k \ll |\mathbf{k}_0|$, it should be clear that the observed spin precession during intervalence transitions is due to the beating between band wave functions that have been coupled by field. This is also confirmed by the magnitude of residual precession frequency, which multiplied by $\hbar$ coincides with the energy difference between the bands at the initial hole wave vector $\mathbf{k}_0$. Thus, the spin transients shown in Figs. 2–5 correspond to wave function beating during vertical interband hole transitions. A more complicated precession pattern may be observed if all three bands are coupled simultaneously by an electric field. This, for example, may happen at intermediate times during excitation of the split-off band by an ultrashort pulse. Due to the stronger coupling coefficient between heavy- and light-mass bands, at intermediate times all bands may appear to be excited simultaneously as Fig. 3 shows [also cf. Fig. 11(a), where the effect is more pronounced].

In describing the Figs. 1 and 2 it was noted that allowed and forbidden transitions may be observed by just changing the sense of rotation of the electric field. However, the classification of the transitions to allowed and forbidden ones is meaningful only if the Hamiltonian and spin operators commute—i.e., when, in the energy-band representation, both the energy and spin are good quantum numbers. This may happen when the spin-orbit interaction is absent or weak as it is for conduction-band electrons. Since in the valence-band case this is not satisfied, in fact, the intermediate transitions are possible too as shown in Fig. 6(a), where the time evolution of the $\langle J_z \rangle$ component from the initial to final value as a function of the band mixing parameter a in Eq. (1) is shown. Here the hole is excited by the same π pulse shown in Fig. 2(a). From Fig. 6(a) it is clear that at $a=0$ the transitions are allowed (in this case the hole initially was in the "first" of the two degenerate bands) and at $a=1$ they are forbidden (in this case the hole initially was in the "second" of the degenerate bands). For intermediate values of a one also gets intermediate $\langle J_z \rangle$ values. In Fig. 6(b) there is plotted the dependence of the initial (at $t=0$) and final (at $t=5$ ps) z projections of the spin as a function of a as well as the dependence of the final probability $p_{l\text{fin}}$ to excite the light-mass band. The points represent calculations similar to those in Fig. 6(a) while the curves represent the empirical formulas

$$\langle J_z \rangle_{\text{ini}} \simeq -\frac{3}{2}(1-2a^2), \qquad (7)$$

$$\langle J_z \rangle_{\text{fin}} \simeq -\frac{1}{2}(1-4a^2), \qquad (8)$$

$$p_{l\text{fin}} \simeq 1-a^2. \qquad (9)$$

Equations (7)–(9) are dependent only on a single parameter a, since the spin projections in [001]-type directions are nearly degenerate; i. e., all $\langle \mathbf{J} \rangle$'s lie on the spin line parallel to k_z axis, Fig. 1. The same relationships were found when the hole was excited from heavy to split-off band by π pulse. As shown in the Appendix, Eqs. (7)–(9) also follow from a simple spherical and parabolic valence-band model. This is
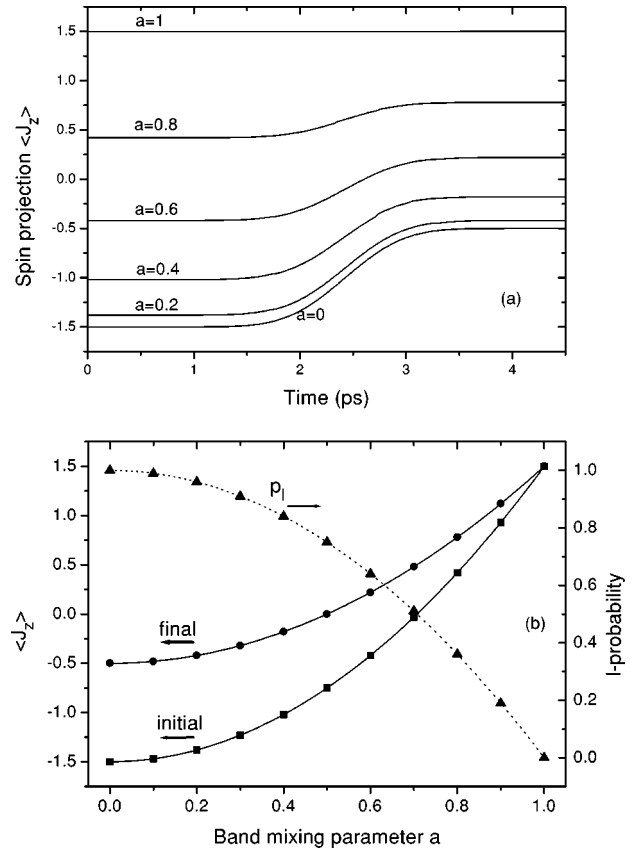

FIG. 6. (a) Switching dynamics of $\langle J_z \rangle$ at various heavy-mass band mixing parameter a values under by π pulse excitation, $\hbar\omega = 9.89$ meV. The curve at $a=0$ coincides with the $\langle J_z \rangle$ curve in Fig. 2(b). (b) Initial, at $t=0$, and final, at $t=5$ ps, spin projections $\langle J_z \rangle$ and the probability to excite the hole in the light-mass band as a function of parameter a.

not surprising, since in the [001] direction of Si the parabolicity of the bands is satisfied to relatively large $\mathbf{k}$'s.

IV. OFF-RESONANCE EXCITATION

In the previous section the exciting frequency satisfied the condition for vertical and resonant transitions between i and j bands: $\hbar\omega = \Delta\varepsilon_{ij}(\mathbf{k}_0)$. Figure 7 shows the time dependence of the probability p_l and spin components, when the initial wave vector was increased by 5% from its resonance value $k_{z0} = 0.378$ nm^{-1} or equivalently the excitation frequency was detuned by 7.3%. The transients in this figure are to be compared with those in Fig. 2 where the initial conditions are identical and only the frequency of the electric field is different. It seen that now the final probabilities to find the hole in the heavy- and light-mass bands after the excitation are close to 0.5. As a result, the precession amplitude of $\langle \mathbf{J} \rangle$ around the z direction, due to the strong beating of the heavy- and light-mass band wave functions, has very large amplitude. Also, it should be noted that the final value of the z component is smaller: $\langle J_z \rangle \approx -1$ rather than $\langle J_z \rangle = -1/2$ at the exact resonance.

In Fig. 8 the open points and the curve show, respectively, computed data and fitting by the Lorentzian curve that rep-
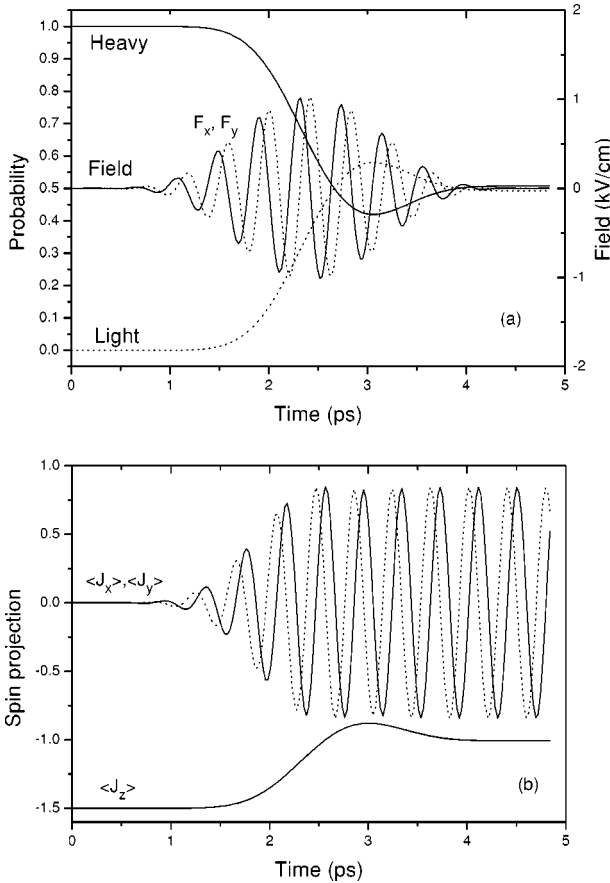
FIG. 7. (a) F_x and F_y components of the circularly polarized electric field and time dependence of the probability to find the hole in heavy- and light-mass bands. The exciting field frequency was detuned by 7.3% from the resonance frequency $\hbar\omega = 9.89$ meV. (b) Time dependence of spin components. The initial spin is $\langle \mathbf{J} \rangle = (0,0,-3/2)$ and $\mathbf{k}_0 \| [001]$. This figure should be compared with Fig. 2.

resents the dependence of the final $\langle J_z \rangle$ on the exciting energy $\hbar\omega$. Also, in the same figure the final p_l as a function of $\hbar\omega$ was plotted for comparison. The width at half maximum is about 1.6 meV for both curves. Strong correlation between
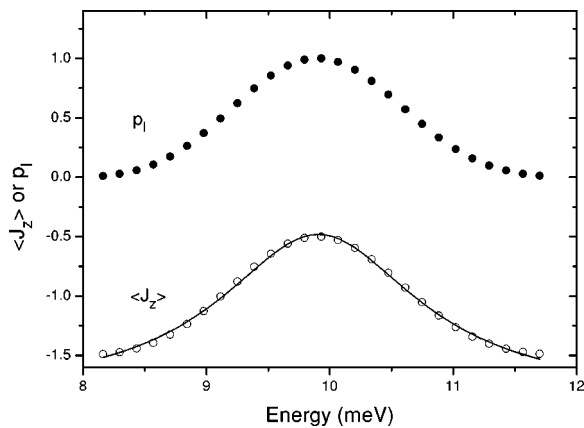
FIG. 8. The final spin projection $\langle J_z \rangle$ and the probability p_l to excite the light-mass band by π-type pulse versus photon energy.
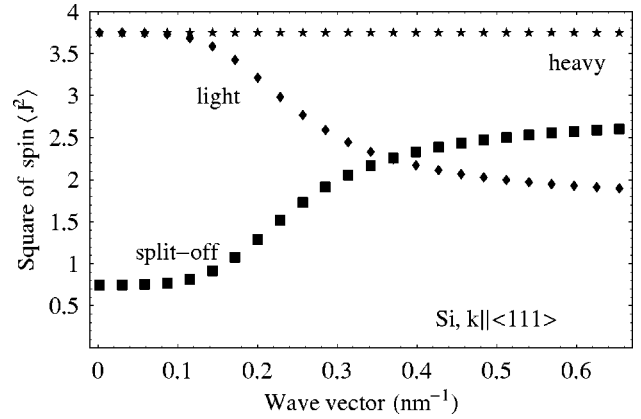
FIG. 9. Dependence of the square of hole spin on the magnitude of wave vector in the $\langle 111 \rangle$ direction for heavy-mass, light-mass, and split-off bands of Si.

bandwidths of the spin and probability resonance curves confirms once more that there exists strong correlation between the spin precession and the heavy- and light-mass band mixing during and after the transition.

V. ULTRASHORT EXCITATION

The condition $\Delta \mathbf{k} \ll \mathbf{k}_0$ for vertical excitation is satisfied if the field amplitude is small. In addition, the field must vary harmonically for excitation to be effective. If ultrashort, shorter than about 1 ps, π-type pulses are used, then $\Delta \mathbf{k}$ becomes comparable to $\mathbf{k}_0$. In this case the interband transitions, strictly speaking, are no longer vertical. Since the interband coupling depends on $\mathbf{k}$—for example, for spherical and parabolic bands it is proportional to $k_\perp / |\mathbf{k}|$, where $k_\perp$ is the component perpendicular to the field[19]—the coupling strength between valence bands may change during excitation by the ultrashort pulse. In addition, at large $\Delta \mathbf{k}$'s the spin surface during excitation may not preserve its shape. Since, in general, the shape depends on the $\mathbf{k}$ length, the spin surface will be pulsating synchronously with $\mathbf{k}(t)$ in this case.

As a measure of the sensitivity of spin to the wave vector length in Fig. 9 the dependence of the square of spin $\langle \mathbf{J}^2 \rangle$ on $\mathbf{k}$ pointing in the $\langle 111 \rangle$ direction, where the deviation from the parabolicity is the strongest, is plotted. At $\mathbf{k}=0$ the valence-band Hamiltonian and the operator $\mathbf{J}$ commute, and one has that $\langle \mathbf{J}^2 \rangle = J(J+1)$ in this limiting case, which gives $\langle \mathbf{J}^2 \rangle = 15/4$ for the heavy- and light-mass bands and $\langle \mathbf{J}^2 \rangle = 3/4$ for the split-off band. Due to strong band nonparabolicity and warping in Si, however, at $|\mathbf{k}| \approx 0.365$ nm^{-1} (this value corresponds to thermal energy 25 meV for the heavy-mass hole), the curves of $\langle \mathbf{J}^2 \rangle$ for light-mass and split-off bands intersect. For other directions of $\mathbf{k}$, effect of nonparabolicity was found to be weaker, especially in the [001] direction. As a consequence of the deformation of spin surfaces at large $\Delta \mathbf{k}$'s, control of spin becomes possible even if interband transitions are forbidden.

To make the control of spin more flexible in the case of ultrashort pulses, the electric field $\mathbf{F}(t)$ in Eq. (4) was approximated by more general formula
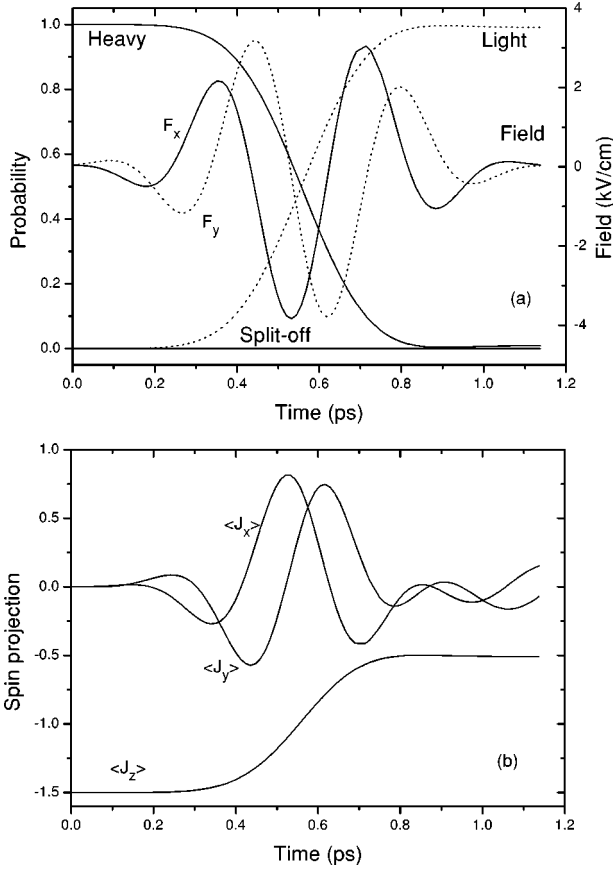
FIG. 10. (a) Ultrashort and optimized π-type electric field pulse $[(F_x, F_y)]$ and the probabilities to find the hole in the heavy-mass, light-mass, and split-off bands vs time. (b) Time dependence of the spin components. The initial spin is $\langle \mathbf{J} \rangle = (0, 0, -3/2)$, $\mathbf{k}_0 \| [001]$.

$$\mathbf{F}(t) = \sum_{i=1}^{2} F_0 \mathbf{e}_i \sin[\omega(t - t_d) + \alpha(t - t_d)^2 + \varphi_i]$$

$$\times \frac{\exp\left(-\sum_{n=2}^{4} a_n \tau^n\right)}{1 + \text{sgn}(t - t_d) a_1 \tau^m}, \qquad (10)$$

where $\mathbf{e}_1$ and $\mathbf{e}_2$ are mutually orthogonal unit vectors and $\tau = (t - t_d)/t_f$. Here, t_d is the delay time and t_f is the final simulation time. In present calculations, the value $t_d = t_f/2$ was used. In formula (10), nine parameters—amplitude F_0, angular frequency ω, chirping coefficient α, initial phases φ_1 and φ_2, and four parameters a_n that control the shape of an envelope function of the field—were varied within some fixed ranges to get an optimal π pulse.

Figures 10(a) and 11(a) show such optimal (or close to optimal) electric field pulses and the resulting time dependence of the probabilities $p_l(t)$ and $p_s(t)$ to detect the hole in the light-mass and split-off bands at the moment t. The field is "circularly" polarized, $\varphi_2 - \varphi_1 = \pi/2$. At $t = 0$ the hole was in the heavy-mass band and possessed the wave vector $\mathbf{k}_0 = 0.378 \times (0, 0, 1)$ nm^{-1}. The spin projections [(b) panels] and the interband probabilities [(a) panels] now are less correlated due to the $\mathbf{k}$ dependence of spin surfaces. The spin switching time for heavy-light transitions now is about 3 ps,
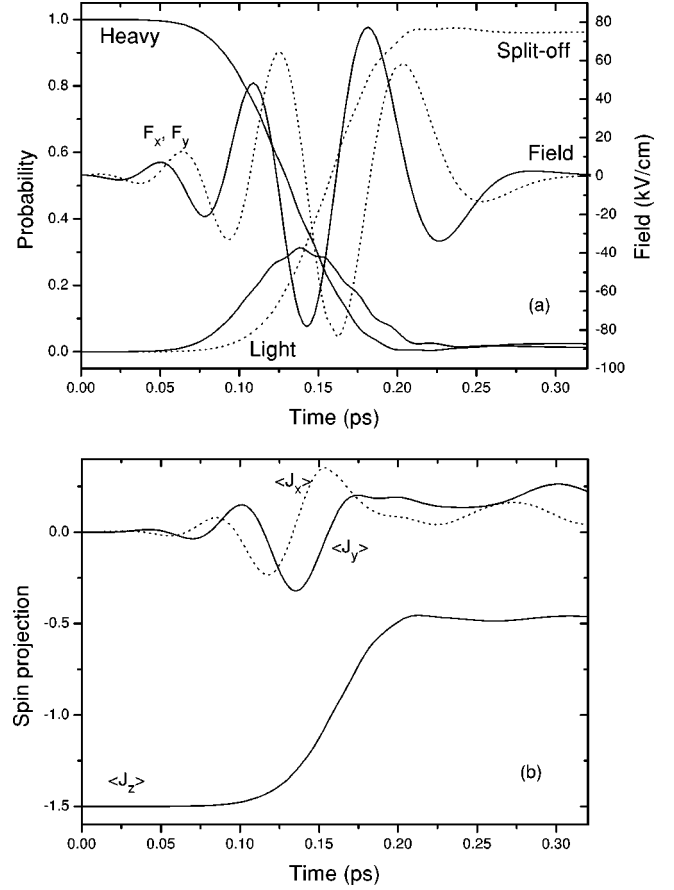

FIG. 11. The same as in Fig. 10, but after optimization of the heavy- split-off transition.

while that for heavy-mass–split-off transitions is about 0.1 ps. Probably, it is possible to achieve shorter switching times if, instead of variable polarity control pulses, monopolar pulses were used in the optimization. In Ref. 20 it was shown that with optimized monopolar electric field pulses the shortest interband population switching time Δt_{ij} between i and j bands is limited by the energy uncertainty relation $\Delta t_{ij} \Delta \varepsilon_{ij} \approx \hbar$. For silicon at $|\mathbf{k}_0| = 0.378$ nm^{-1} one has $\Delta \varepsilon_{hl} = 9.89$ meV and $\Delta \varepsilon_{hs} = 50.1$ meV, which gives $\Delta t_{hl} \approx 0.4$ ps and $\Delta t_{hs} \approx 0.08$ ps.

Finally, in connection with the wave vector equation (4) the following point should be noted. At large $\Delta \mathbf{k}$'s the final $\mathbf{k}$ may or may not coincide with the initial one. In Figs. 10 and Fig. 11, the optimized pulse has nearly equal positive and negative areas under the electric field curve; as a result, at the end of the pulse the wave vector returns back to its initial position. Such transitions may be called quasivertical. If the dissipation and wave function dephasing mechanisms come into play, the vertical, when $\Delta \mathbf{k} \ll \mathbf{k}_0$, and quasivertical, when $\Delta \mathbf{k} \sim \mathbf{k}_0$, transitions may experience different perturbations, due to the $\mathbf{k}$ dependence of spin relaxation and dephasing times.

VI. DISCUSSION AND CONCLUSIONS

In this section, differences between electron and hole spin properties that follow from this study are discussed briefly.

Spin degeneracy. Complex valence-band structure entails a much richer spectrum of the hole spin transitions. In the case of electrons, the control of spin usually takes place on a single spin surface of spherical symmetry where an electron "spintronics theater" is played.[21] The valence band for this purpose has three "stages" or spin surfaces of different form. From the practical point of view the most important are the transitions of the ballistic holes between the spin surfaces of heavy- and light-mass bands. For these holes, due to the large density of states in the heavy-mass band, the dominant contribution will come from the spin surfaces that have cigar form in the direction of the hole movement. In particular, in [001]-type directions, where spin surfaces are characteristic of parabolic bands for relatively large $\mathbf{k}$'s (cf. Fig. 9), the degeneracy of spin states will be the largest. This means that the ensemble of the ballistic holes moving in the [001]-type direction may have a very small deviation from the ideal case, where all spins are pointing in the same or nearly the same direction.[22] This relaxes the stringent matching conditions that should be satisfied between three-dimensional spin surfaces in real spin devices. By the same reason, a strong spin degeneracy of [001]-type holes will favor an efficient injection of ballistic holes, the spins of which are perpendicular to (001)-type injection plane. If the spins are aligned in the injection plane, free propagation of the hole in a direction perpendicular to the injection plane will be forbidden, since the heavy-hole states should satisfy the condition $\langle \mathbf{J} \rangle \| \mathbf{k}$, at least at not too large $\mathbf{k}$'s. This may explain why it was possible experimentally to achieve high spin injection efficiency using [100] oriented holes[23] and to observe large anisotropy in electrical spin injection efficiency between spins parallel and perpendicular to the injection plane in ferromagnetic semiconductor heterostructures.[24]

Hole spin precession. In the presence of a magnetic field the quantum mechanical origin of spin precession is the beating between wave functions of two nearly degenerate energy levels. Since the beating frequency is proportional to the difference between energies of levels in atoms or bands in solids, the precession frequency can be controlled by a magnetic field. In the spin transistor[25] the splitting between nearly degenerate levels is controlled by an electric field, which in conjunction with electron ballistic movement allows us to create a spatial screw of the electron spin, the pitch of which depends on the strength of the electric field. In the valence band of elemental semiconductors the precession is caused by beating between heavy-mass, light-mass, and split-off bands. Therefore, the precession mechanism is different from the mentioned precession between two nearly spin-degenerate levels or bands. The degeneracy of heavy-mass, light-mass, or split-off bands, in principle, may also give an additional, low-frequency beating and the resulting precession. However, during ultrafast interband transitions, where the switching time is close to the reciprocal interband uncertainty energy, the low-frequency precession caused by degenerate bands will be of minor importance.

As mentioned, in case of nearly degenerate electron levels the vector $\langle \mathbf{J} \rangle$ rotates (precesses) on a single spin surface. In the case of valence bands the precession takes place between different spin surfaces. In a sense, hole precession in the

tetrahedral semiconductors is more akin to the beating between heavy- and light-mass band excitons found in the luminescence experiments on III-V compounds.[26] Because of a different mechanism, the hole precession trajectory should not necessarily be a circle on the spin surface as it is in electron case. This is the reason why very complicated hole spin precession trajectories could be observed for some directions of $\mathbf{k}_0$ and arbitrary values of the parameters a and ϕ that determine the initial spin, especially when all three valence-bands are excited simultaneously by an ultrashort pulse. Due to complex valence-band structure, additional numerical experiments are required to gain a better understanding of the optimal initial conditions and how to perform a smooth switching of an ensemble of spins between initial and final states.

Spin control. As follows from this investigation coherent control of hole spins in Si is associated with both the intervalence and intravalence hole transitions. The first mechanism is due to the coupling between different spin surfaces at some fixed $\mathbf{k}$, while the second one is due to the dependence of the shape of the spin surface on the length of $\mathbf{k}$. For spherical and parabolic bands the spin is independent of the magnitude of $\mathbf{k}$. Nonetheless, the control of spin is possible in this case if the electric field changes the direction of the hole wave vector. The latter mechanism should be very effective for heavy holes, the spin of which is very close to the direction of the hole movement. However, in real semiconductors, because of band warping and nonsphericity, in addition, the intravalence spin control method based on deformation of spin surfaces as the magnitude of $\mathbf{k}$ is changed is possible too.

Of the above-mentioned spin control methods, the most promising one is associated with hole intervalence transitions. In this case spin switching by π pulses can be achieved on heavy- light or heavy-split-off band transitions excited either by harmonic or wideband ultrashort pulses. If the energy of the hole is smaller than the optical phonon energy, as shown in Ref. 27, the free-of-flight length of the injected hole may be as long as 0.3 μm. In this case long harmonic π pulses can be used to control the hole spin during its flight. In the opposite case, due to a strong hole coupling to optical phonons, the hole spin lifetime may be very short, about 0.1 ps.[10] Coherent control of hole spin in this case may be achieved by ultrashort and specially tailored electric pulses. The use of such pulses may be advantageous from different considerations too. As Fig. 8 shows the excitation of spins by long π pulses is selective, and at high lattice temperature the coherence of such an excitation will be destroyed by phonon- or impurity-related spin relaxation mechanisms. However, the coherence properties will be preserved under ultrashort π pulse excitation. In addition, due to the wide bandwidth of such pulses, a larger number of spins may be excited simultaneously. To have an ultrafast and smooth—i.e., precessionless—spin switching, the shape of the ultrashort pulse must be optimized beforehand.

In conclusion, the paper shows that the most important properties of the hole spin may be explained by hole spin surfaces for individual bands. The dynamics of hole spin in time-dependent electric fields may be viewed and analyzed as transitions on or between such surfaces. Using this ap-

proach, various intraband and interband spin control mechanisms were proposed which can be applied in the semiconductor spintronics. The coherent switching time of hole spin in Si was found to be shorter than a picosecond for heavy-light transitions and a hundred of femtoseconds for heavy-split-off transitions.

APPENDIX: HOLE SPIN IN THE SPHERICAL AND PARABOLIC TWO-BAND MODEL

In the limiting case of a strong spin-orbit interaction, when the split-off band does not participate in the intervalence transitions, spherical and parabolic heavy- and light-mass bands can be described by the following two-band Hamiltonian:[16]

$$H_{LK} = \frac{\mathbf{k}^2}{2}\left(\gamma_1 + \frac{5}{2}\gamma\right) - \gamma(\mathbf{Jk})^2, \tag{A1}$$

where γ and γ_1 are two constants related to the heavy and light masses of the hole:

$$m_l = (\gamma_1 + 2\gamma)^{-1}, \tag{A2}$$

$$m_h = (\gamma_1 - 2\gamma)^{-1}. \tag{A3}$$

In this approximation the matrices of the total angular momentum have the form

$$J_x = \begin{vmatrix} 0 & \dfrac{i\sqrt{3}}{2} & 0 & 0 \\ -\dfrac{i\sqrt{3}}{2} & 0 & i & 0 \\ 0 & -i & 0 & \dfrac{i\sqrt{3}}{2} \\ 0 & 0 & -\dfrac{i\sqrt{3}}{2} & 0 \end{vmatrix}, \tag{A4}$$

$$J_y = \begin{vmatrix} 0 & \dfrac{\sqrt{3}}{2} & 0 & 0 \\ \dfrac{\sqrt{3}}{2} & 0 & 1 & 0 \\ 0 & 1 & 0 & \dfrac{\sqrt{3}}{2} \\ 0 & 0 & \dfrac{\sqrt{3}}{2} & 0 \end{vmatrix}, \tag{A5}$$

$$J_z = \begin{vmatrix} \dfrac{3}{2} & 0 & 0 & 0 \\ 0 & \dfrac{1}{2} & 0 & 0 \\ 0 & 0 & -\dfrac{1}{2} & 0 \\ 0 & 0 & 0 & -\dfrac{3}{2} \end{vmatrix}. \tag{A6}$$

The unitary transformation matrix

$$T = \frac{\sin\theta}{2\sqrt{2}}\begin{vmatrix} -ce^{-i\varphi} & c^*e^{-i\varphi} & \sqrt{3}e^{-i\varphi} & -\sqrt{3}e^{-i\varphi} \\ -\sqrt{3} & -\sqrt{3} & -c^* & -c \\ \sqrt{3}e^{i\varphi} & -\sqrt{3}e^{i\varphi} & c^*e^{i\varphi} & -ce^{i\varphi} \\ ce^{i2\varphi} & c^*e^{i2\varphi} & -\sqrt{3}e^{i2\varphi} & -\sqrt{3}e^{i2\varphi} \end{vmatrix}, \tag{A7}$$

where $c = 1 + i2\cot\theta$, brings the Hamiltonian (A1) to a diagonal form. The angles θ and φ are polar angles of the wave vector $\mathbf{k} = (k\sin\theta\cos\varphi, k\sin\theta\sin\varphi, k\cos\theta)$. After the transformation $\mathcal{J}_i = T^\dagger J_i T$, the matrices (A4)–(A6) in the energy representation become

$$\mathcal{J}_x = \begin{vmatrix} 0 & \dfrac{3}{2}S_e\cos\varphi & \dfrac{\sqrt{3}}{2}\sin\varphi & i\dfrac{\sqrt{3}}{2}C_e\cos\varphi \\ \dfrac{3}{2}S_e^*\cos\varphi & 0 & -i\dfrac{\sqrt{3}}{2}C_e^*\cos\varphi & -\dfrac{\sqrt{3}}{2}\sin\varphi \\ \dfrac{\sqrt{3}}{2}\sin\varphi & i\dfrac{\sqrt{3}}{2}C_e\cos\varphi & \sin\varphi & -i\dfrac{1}{2}(1 + C_e)\cos\varphi \\ -i\dfrac{\sqrt{3}}{2}C_e^*\cos\varphi & -\dfrac{\sqrt{3}}{2}\sin\varphi & i\dfrac{1}{2}(1 + C_e^*)\cos\varphi & -\sin\varphi \end{vmatrix}, \tag{A8}$$

$$\mathcal{J}_y = \begin{vmatrix} 0 & \frac{3}{2}S_e\sin\varphi & -\frac{\sqrt{3}}{2}\cos\varphi & i\frac{\sqrt{3}}{2}C_e\sin\varphi \\ \frac{3}{2}S_e^*\sin\varphi & 0 & -i\frac{\sqrt{3}}{2}C_e^*\sin\varphi & \frac{\sqrt{3}}{2}\cos\varphi \\ -\frac{\sqrt{3}}{2}\cos\varphi & i\frac{\sqrt{3}}{2}C_e\sin\varphi & -\cos\varphi & -i\frac{1}{2}(1+C_e)\sin\varphi \\ -i\frac{\sqrt{3}}{2}C_e^*\sin\varphi & \frac{\sqrt{3}}{2}\cos\varphi & i\frac{1}{2}(1+C_e^*)\sin\varphi & \cos\varphi \end{vmatrix}, \tag{A9}$$

$$\mathcal{J}_z = \begin{vmatrix} 0 & \frac{3}{2}C_e & 0 & -i\frac{\sqrt{3}}{2}S_e \\ \frac{3}{2}C_e^* & 0 & i\frac{\sqrt{3}}{2}S_e^* & 0 \\ 0 & -i\frac{\sqrt{3}}{2}S_e & 0 & -\frac{1}{2}(1-iS_e) \\ i\frac{\sqrt{3}}{2}S_e^* & 0 & -\frac{1}{2}(1+iS_e^*) & 0 \end{vmatrix}, \tag{A10}$$

where $S_e = \sin\theta\exp(i\theta)$ and $C_e = \cos\theta\exp(i\theta)$. The Hamiltonian (A1) after the transformation is diagonal in the order $(\varepsilon_h, \varepsilon_h, \varepsilon_l, \varepsilon_l)$, where $\varepsilon_{h,l} = \mathbf{k}^2/2m_{h,l}$.

Using the parametric form of the state vector, $f_h = (a_h, \sqrt{1-a_h^2}\exp(i\phi_h), 0, 0)$, the following average values of the angular momentum for heavy-mass hole, $\langle\mathbf{J}\rangle_h = (\langle J_x\rangle_h, \langle J_y\rangle_h, \langle J_z\rangle_h)$, are found with the help of Eqs. (A8)–(A10)

$$\langle J_x\rangle_h = \frac{3}{2}\sin 2\vartheta_h\cos(\theta-\phi_h)\sin\theta\cos\varphi, \tag{A11}$$

$$\langle J_y\rangle_h = \frac{3}{2}\sin 2\vartheta_h\cos(\theta-\phi_h)\sin\theta\sin\varphi, \tag{A12}$$

$$\langle J_z\rangle_h = \frac{3}{2}\sin 2\vartheta_h\cos(\theta-\phi_h)\cos\theta, \tag{A13}$$

where the parameter a_h was replaced by new parameter $\cos\vartheta_h$. From Eqs. (A11)–(A13) it should be clear that the vector $\langle\mathbf{J}\rangle_h$ is parallel to $\mathbf{k}$ in spherical and parabolic band approximation. The magnitude of $\langle\mathbf{J}\rangle_h$ depends on the polar angle θ of $\mathbf{k}$ and degenerate band mixing through parameters a_h (or ϑ) and ϕ_h. All values of $|\langle\mathbf{J}\rangle_h|$ are possible between $\pm\frac{3}{2}$. Therefore, for simple valence bands the total angular momentum of the heavy hole is either parallel or antiparallel to $\mathbf{k}$, or equal to zero. This property may be responsible for the anisotropy in the injection efficiency of the ballistic spins into intrinsic semiconductors from a planar contact fabricated from, for example, a diluted magnetic semiconductor. For real bands the spin surfaces will be cigar shaped;[11,22] as a result, the anisotropy will be smaller.

Similar calculations for light-mass holes with $f_l = (0, 0, a_l, \sqrt{1-a_l^2}\exp(i\phi_l))$ yield the following projections of $\langle\mathbf{J}\rangle_l$:

$$\langle J_x\rangle_l = \frac{1}{4}\cos 2\vartheta_l\{-4\sin\varphi + (\sin(2\theta-\phi_l) - 3\sin\phi_l)\tan 2\vartheta_l\cos\varphi\}, \tag{A14}$$

$$\langle J_y\rangle_l = \frac{1}{4}\cos 2\vartheta_l\{4\cos\varphi + [\sin(2\theta-\phi_l) - 3\sin\phi_l]\tan 2\vartheta_l\sin\varphi\}, \tag{A15}$$

$$\langle J_z\rangle_l = \frac{1}{4}\sin 2\vartheta_l[\cos(2\theta-\phi_l) - 3\cos\phi_l], \tag{A16}$$

where a_l was replaced by $\cos\vartheta_l$. Eqs. (A14)–(A16) describe the ellipsoid of revolution (spheroid), the minor axis of which is parallel to $\mathbf{k}$ and equals $\frac{1}{2}$. The other two principal axes are equal 1. Thus, the injection of light-hole ballistic spin should be anisotropic too, although the anisotropy is expected to be smaller in this case and have an opposite sign.

If, as Fig. 1 shows, Eqs. (A11)–(A16) are plotted parametrically in three-dimensional spin space as a function of (ϑ_h, ϕ_h) or (ϑ_l, ϕ_l), one will obtain geodesic lines, the family of which will represent the corresponding spin surface. For different parametrizations of the heavy- and light-hole states one will have different families of geodesic lines. However, all families will lie on the same spin surface, the overall shape of which in this simple model depends only on polar angles θ and φ of the wave vector. If the bands are nonparabolic and nonspherical or the split-off band is included, the

shape of the surface, in addition, will depend on the modulus of **k** and the direction with respect to the crystallographic axes. For these more complex bands the spin surfaces could be found only numerically. From the practical point of view it should be noted that for those **k**'s that are pointing in the high-symmetry directions the numerical results, depending on the numerical algorithm used to find the transformation matrix between the energy and spin representations, may be unstable, in a sense that the spin surface may align along one of the high-symmetry wave vectors within the star to which a given **k** belongs. The instability is associated with the high symmetry of the problem and the nonuniqueness of the transformation matrix that diagonalizes the Hamiltonian. On this occasion I would like to point out that the wave vector in the tables and figures of the Ref. 11 should be interpreted as belonging to a corresponding wave vector star. The exact correspondence between **k** and the spin surfaces presented in this article can be obtained after interchange: $J_x \rightarrow -J_y$, $J_y \rightarrow J_x$, or $k_x \rightarrow -k_y$, $k_y \rightarrow k_x$.

In addition, it was found that, depending on the algorithm used, the numerical transformation may also effect the shape of the trajectories of geodesic lines on the spin surface, although the overall form of the spin surface densely covered by the geodesic lines was found to be uninfluenced in all cases. For example, the Cartesian coordinates of the initial and final spins in Eqs. (A13) and (A16) which follow from the analytical calculations and in Eqs. (7) and (8) which follow from numerical calculations, in fact, represent different parametrizations on the same spin surface. Eqs. (A13) and (A16) can be transformed into Eqs. (7) and (8) by changing the parametrization in the following way: $a_{h,l} \rightarrow (1 \pm 2a\sqrt{1-a^2} \cos \phi)^{1/2}/\sqrt{2}$. Although the parametrization of the band states is not unique, however, it should be stressed once more that the spin surfaces calculated by parametrized wave functions were found to be very useful objects in all cases in understanding of and in modeling very complicated spin transitions within the valence subband.

Finally, it should be noted that, if the analysis is restricted to a simple 4×4 two-band valence Hamiltonian, the matrix of total angular momentum **J** and spin **S**, apart from the factor of 3, will have the same structure.[28] This means that the results of this appendix are applicable to hole intrinsic spin **S** as well. However, in a more general case the dynamical properties of **J** and **S** will be different.

*Electronic address: dargys@pfi.lt

[1] S. A. Wolf, D. D. Awschalom, R. A. Buhrman, J. M. Daughton, S. von Molnár, M. L. Roukes, A. Y. Chtchelkanova, and D. M. Treger, Science **294**, 1488 (2001).

[2] J. F. Gregg, I. Petej, E. Jouguelet, and C. Dennis, J. Phys. D **35**, R121 (2002).

[3] I. Žutić, J. Fabian, and S. Das Sarma, Rev. Mod. Phys. **76**, 323 (2004).

[4] G. Fishman and G. Lampel, Phys. Rev. B **16**, 820 (1977).

[5] A. Bournel, P. Dollfus, E. Cassan, and P. Hesto, Appl. Phys. Lett. **77**, 2346 (2000).

[6] Pil Hun Song and K. W. Kim, Phys. Rev. B **66**, 035207 (2002).

[7] W. Kauschke, N. Mestres, and M. Cardona, Phys. Rev. B **35**, 3843 (1987).

[8] P. Langot, R. Tommasi, and F. Vallée, Phys. Rev. B **54**, 1775 (1996).

[9] K. C. Burr and C. L. Tang, Appl. Phys. Lett. **74**, 1734 (1999).

[10] D. J. Hilton and C. L. Tang, Phys. Rev. Lett. **89**, 146601 (2002).

[11] A. Dargys, Phys. Status Solidi B **241**, 145 (2004).

[12] A. Dargys and P. Harrison, Semicond. Sci. Technol. **18**, 247 (2003).

[13] A. Dargys, IEEE J. Sel. Top. Quantum Electron. **10**, 155 (2004).

[14] A. Dargys, Phys. Rev. B **66**, 165216 (2002).

[15] J. M. Luttinger and W. Kohn, Phys. Rev. **97**, 869 (1955).

[16] J. M. Luttinger, Phys. Rev. **102**, 1030 (1956).

[17] B. A. Foreman, J. Phys.: Condens. Matter **12**, R435 (2000).

[18] A. Baldereschi and N. Lipari, Phys. Rev. B **8**, 2697 (1973).

[19] A. Dargys and A. F. Rudolph, Phys. Status Solidi B **140**, 535 (1987).

[20] A. Dargys, Phys. Rev. B **64**, 235123 (2001).

[21] D. M. Sullivan and D. S. Citrin, J. Appl. Phys. **94**, 6518 (2003).

[22] A detailed study of the spin surfaces in A_3B_5 semiconductors at large **k**'s shows that in these semiconductors the heavy-hole spins are nearly parallel to **k**, if **k**‖[001] or **k**‖[111]: A. Dargys, Phys. Status Solidi B (to be published).

[23] Y. Ohno, D. K. Young, B. Beschoten, F. Matsukura, H. Ohno, and D. D. Awschalom, Nature (London) **402**, 790 (1999).

[24] D. K. Young, E. Johnston-Halperin, D. D. Awschalom, Y. Ohno, and H. Ohno, Appl. Phys. Lett. **80**, 1598 (2003).

[25] S. Datta and B. Das, Appl. Phys. Lett. **56**, 665 (1990).

[26] J. Shah, *Ultrafast Spectroscopy of Semiconductors and Semiconductor Nanostructures* (Springer-Verlag, Berlin, 1999).

[27] D. Sprinzak, M. Heiblum, Y. Levinson, and H. Shtrikman, Phys. Rev. B **55**, R10185 (1997).

[28] M. Abolfath, T. Jungwirth, J. Brum, and A. H. MacDonald, Phys. Rev. B **63**, 054418 (2001).